PHILOSOPHICAL TRANSACTIONS OF THE ROYAL SOCIETY A MATHEMATICAL, PHYSICAL & ENGINEERING SCIENCES

A comparison of Navier-Stokes solutions with the theoretical description of unsteady separation

Kevin W. Cassel

Phil. Trans. R. Soc. Lond. A 2000 **358**, 3207-3227
doi: 10.1098/rsta.2000.0705

10.1098/rsta.2000.0705

THE ROYAL SOCIETY

A comparison of Navier–Stokes solutions with the theoretical description of unsteady separation

By Kevin W. Cassel

Fluid Dynamics Research Center,
Mechanical, Materials and Aerospace Engineering Department,
Illinois Institute of Technology, Chicago, IL 60616, USA

Numerical solutions of the unsteady two-dimensional boundary-layer and Navier–Stokes equations are considered for the flow induced by a thick-core vortex above an infinite plane wall in an incompressible flow. Vortex-induced flows of this type generally involve unsteady separation, which results in an eruption of high-vorticity fluid within a narrow streamwise region. At high Reynolds numbers, the unsteady separation process is believed to pass through a series of asymptotic stages. The first stage is governed by the classical non-interactive boundary-layer equations, for which solutions are given, and terminate in the Van Dommelen singularity. As an eruption develops, the boundary layer thickens and provokes a viscous–inviscid interaction leading to the second stage of unsteady separation. The third stage occurs when the normal pressure gradient becomes important locally within the boundary layer. In order to identify these asymptotic stages at large, but finite, Reynolds numbers, solutions of the full Navier–Stokes equations are obtained for the flow induced by a thick-core vortex. These results generally support this sequence of events; however, a large-scale viscous–inviscid interaction is found to begin at a time much earlier than allowed for by the asymptotic theory; that is it begins to occur prior to the formation of a spike within the boundary layer. Some consequences of these results on our understanding of unsteady separation are discussed.

Keywords: unsteady separation; viscous–inviscid interaction; Navier–Stokes solutions

1. Introduction

A boundary layer subject to an adverse streamwise pressure gradient is susceptible to unsteady separation, which is characterized by a sharp spike that erupts into the outer inviscid flow. This adverse pressure gradient may be due to the surface geometry, as in the case of the flow around a circular cylinder or near the leading edge of an aerofoil, or it may be due to the presence of a vortex convecting near a surface. Unsteady separation occurs in many technologically important flows including dynamic stall, juncture flows and turbulent boundary layers (see Doligalski *et al.* (1994), and the references cited therein). Because unsteady eruptive events of this kind are common in a wide variety of high-Reynolds-number flows, a detailed

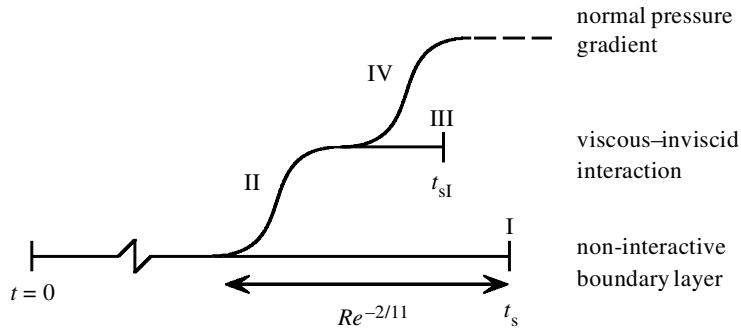

Figure 1. Schematic of the initial asymptotic stages of unsteady separation.

theoretical description of unsteady separation and an understanding of the physical processes involved has been sought for several decades.

At high Reynolds numbers, two-dimensional incompressible flows undergoing unsteady separation are believed to pass through a series of asymptotic stages, each of which involves its own unique scales and is governed by a subset of the Navier–Stokes equations. The first three stages have been identified and are shown schematically in figure 1. The initial stage, represented by the bottom tier in figure 1, is governed by the non-interactive boundary-layer equations. During this stage the adverse pressure gradient imposed across the boundary layer induces the formation of a recirculating-flow region that grows in streamwise and normal extent with time. This non-interactive stage ends abruptly in the Van Dommelen (1981) singularity involving dramatic growth in the displacement thickness and normal velocity in a narrow streamwise region on the upstream side of the recirculation region. The non-interactive boundary-layer singularity occurs at a finite time, t_s, and is denoted by I in figure 1. Van Dommelen & Shen (1982) and Elliott *et al.* (1983) provide an analytical description of this singularity in the form of a local similarity solution within the spike as the singularity is approached; this solution will be referred to here as the terminal boundary-layer solution. One important feature of the terminal solution is that it is independent of the precise form of the adverse pressure gradient that initiated the unsteady separation process; therefore, it has been regarded as a generic structure through which all two-dimensional incompressible separated flows pass. Numerical confirmation of the terminal solution and the non-interactive singularity in two model problems, the impulsively started circular cylinder and the rectilinear vortex above a plane wall, has been given by Van Dommelen & Shen (1980) and Peridier *et al.* (1991*a*). These solutions, which were performed in Lagrangian coordinates, built upon the earlier work of Walker (1978), Doligalski & Walker (1984) and Ece *et al.* (1984), who performed calculations of the unsteady boundary-layer equations using the traditional Eulerian formulation.

The second stage of unsteady separation involves interaction between the boundary layer and the outer inviscid flow which inevitably occurs as the boundary layer thickens locally; this stage is represented by the second tier in figure 1. Elliott *et al.* (1983) have formulated this so-called *first* interactive stage that governs events locally on times of $O(Re^{-2/11})$ surrounding the non-interactive singularity time t_s; the beginning of this stage is labelled II in figure 1. Numerical solutions of this

stage have been obtained in Lagrangian coordinates by Cassel *et al.* (1996) which show that the *first* interactive stage contains a high-frequency inviscid instability resulting in an immediate breakdown at the very onset of interaction. A linear stability analysis revealed that velocity profiles in the initial condition for this stage, which is the terminal boundary-layer solution, are unstable. The consequences of these results were unclear at the time, but they do suggest that some physical influence (possibly interaction) must become important at a time prior to the time-scale on which the *first* interactive stage was thought to act. An alternative approach in which to consider the influence of viscous–inviscid interaction is to use interacting boundary-layer theory, which assumes a large, but finite, Reynolds number and couples the unsteady boundary-layer equations with an interaction condition. Solutions obtained by Peridier *et al.* (1991*b*) for the rectilinear vortex above a plane wall using the Lagrangian formulation of interacting boundary-layer theory show that a singularity occurs within a finite time according to the theory of Smith (1988). This interacting boundary-layer singularity is denoted by III in figure 1 and occurs at t_{sI}. Breakdown occurs when the streamwise pressure gradient and wall shear stress become singular, and at a time prior to that at which the non-interactive singularity occurs, i.e. $t_{\mathrm{sI}} < t_{\mathrm{s}}$. Hoyle & Smith (1994) have considered the three-dimensional form of the interacting boundary-layer singularity.

The third stage of unsteady separation, represented by the third tier in figure 1, has been proposed by Hoyle *et al.* (1991) and considered in more detail by Li *et al.* (1998). In this stage the normal pressure gradient becomes important locally within the boundary layer in order to relieve the interacting boundary-layer singularity; this is indicated by IV in figure 1. The onset of normal pressure gradients within the boundary layer is accompanied by the formation of a nonlinear critical layer that develops near an inflection point in the velocity profiles and results in vortex roll-up near the point of maximum streamwise pressure gradient.

The theoretical description of unsteady separation given above has been pieced together through careful consideration of subsets of the Navier–Stokes equations as the Reynolds number goes to infinity and through interacting boundary-layer theory. While this approach has provided a great deal of insight into the relevant physical processes that occur in unsteady separation at high Reynolds numbers, recent work (in particular by Cassel *et al.* (1996)) has raised some fundamental questions that may be answered more readily using a different approach. In addition, it would be instructive to evaluate the current theoretical description of unsteady separation from an alternative point of view. To these ends, the objective of the present investigation is to provide highly resolved, high-Reynolds-number solutions of the Navier–Stokes equations for the unsteady separation induced by a vortex above a surface in order to confirm the theoretical stages of unsteady separation outlined above and to determine the physical processes that occur prior to the onset of the *first* interactive stage. Other authors have obtained solutions of the unsteady Navier–Stokes equations for flows involving separation (see, for example, Orlandi 1990; Koumoutsakos & Leonard 1995; Choudhuri & Knight 1996; Brinkman & Walker 1996; Dodia *et al.* 1997), but the Reynolds numbers have not typically been large enough to observe the sharp spike that occurs in unsteady separation at high Reynolds numbers. The Navier–Stokes solutions obtained in this investigation do exhibit the small-scale spike and are consistent with the presence of the three stages described above; however, a large-scale viscous–inviscid interaction is found to begin prior to the formation

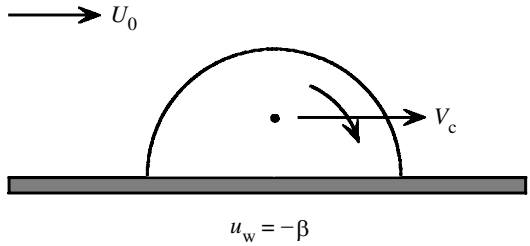

Figure 2. Schematic of the thick-core vortex.

of a spike, which was thought to be a precursor to the onset of interaction. The implications of these results on our understanding of unsteady separation will be discussed.

2. Thick-core vortex

In previous studies of unsteady boundary-layer separation induced by a vortex, the model problem has been one of a rectilinear vortex above an infinite plane wall (see, for example, Walker 1978; Peridier *et al.* 1991*a*). The rectilinear vortex represents a limiting case in two-dimensional vortex flows in which the vorticity is singular and concentrated in a small core. This does not create any difficulties in boundary-layer calculations because the quantity required from the inviscid solution to perform the boundary-layer calculation is the streamwise pressure gradient (or slip velocity) along the surface, and the vortex core, which remains in the inviscid flow, is not calculated. However, in this investigation it is of interest to calculate the Navier–Stokes equations in the entire flow field including the flow within the vortex itself. Therefore, it is advantageous to consider another limiting case of two-dimensional vortex motions, i.e. the so-called thick-core vortex shown schematically in figure 2. The inviscid flow due to the thick-core vortex is described by Batchelor (1967) and consists of a semi-circular vortex, in which the vorticity is proportional to the stream-function, surrounded by the irrotational flow past a circular cylinder in a uniform flow.

The vortex has a velocity V_c relative to the wall due to its self-induced flow and the oncoming uniform flow. Note that $V_c < 0$ for a vortex with negative rotation, as shown in figure 2, in a stagnant flow ($U_0 = 0$). We define a fractional convection rate for the vortex as

$$\alpha = V_c/U_0. \tag{2.1}$$

Therefore, $\alpha = 0$ corresponds to a vortex with sufficient self-induced velocity to balance the uniform flow exactly and remain stationary relative to the wall. As $\alpha \to 1$, the vortex becomes weak and/or far from the wall and convects with the uniform flow speed U_0. For $\alpha < 0$, the vortex is sufficiently strong and/or close to the wall to overcome the oncoming uniform flow and convect upstream.

In a frame of reference moving with the vortex, the centre of the vortex remains stationary, and the wall moves with speed $u_w^* = -V_c = -\alpha U_0$, and the streamwise velocity at infinity becomes $U_0(1 - \alpha)$. Here, and throughout, a variable with an asterisk indicates a dimensional variable. In a frame of reference moving with the

vortex, therefore, the streamfunction is given in cylindrical coordinates (r^*, θ^*) by

$$\psi^* = U_0(1-\alpha)\left(r^* - \frac{e^2}{r^*}\right)\sin\theta^*, \quad r^* > e, \tag{2.2 a}$$

$$\psi^* = 2U_0(1-\alpha)\frac{J_1(kr^*)}{kJ_0(ke)}\sin\theta^*, \qquad r^* \leqslant e, \tag{2.2 b}$$

where the origin is on the surface immediately below the centre of the vortex, and the radius of the semicircular region containing the vorticity has been taken as e for convenience. Note that the solution (2.2 *a*) for $r^* > e$ is the inviscid flow about a circular cylinder of radius e in a uniform flow U_0. In equation (2.2 *b*), J_0 and J_1 are Bessel functions, and k is such that $J_1(ke) = 0$. We define $\lambda = ke$, and take λ to be the first (smallest) zero of J_1 in order to give a single-celled vortex, and from Abramowitz & Stegun (1964) $\lambda = 3.831\,71$. The centre of the vortex is located at the point where $v_\theta^* = -\partial\psi^*/\partial r^* = 0$ along the line $\theta^* = \pi/2$. From equation (2.2 *b*) this occurs where $J_1'(kr_0) = 0$, where r_0 is the normal distance from the surface to the centre of the vortex. From Abramowitz & Stegun (1964), $kr_0 = 1.841\,18$; therefore, the vortex centre is located at $r^* = r_0 = 0.480\,511e$, $\theta^* = \pi/2$.

Taking r_0 to be the characteristic length and the velocity at infinity, $U_0(1-\alpha)$, to be the characteristic velocity, we non-dimensionalize as follows:

$$r = r^*/r_0, \tag{2.3 a}$$

$$\theta = \theta^*, \tag{2.3 b}$$

$$v_r = \frac{v_r^*}{U_0(1-\alpha)}, \tag{2.3 c}$$

$$v_\theta = \frac{v_\theta^*}{U_0(1-\alpha)}, \tag{2.3 d}$$

where v_r and v_θ are the velocity components in the r and θ directions, respectively. The streamfunction in cylindrical coordinates is defined by

$$v_r = \frac{1}{r}\frac{\partial\psi}{\partial\theta}, \tag{2.4 a}$$

$$v_\theta = -\frac{\partial\psi}{\partial r}; \tag{2.4 b}$$

therefore, the non-dimensional streamfunction is

$$\psi = \left[r - \frac{1}{r}\left(\frac{e}{r_0}\right)^2\right]\sin\theta, \quad r > e/r_0, \tag{2.5 a}$$

$$\psi = \frac{2}{r_0}\frac{J_1(kr_0 r)}{kJ_0(ke)}\sin\theta, \qquad r \leqslant e/r_0. \tag{2.5 b}$$

Note that the inviscid stagnation points on the wall are located at $r = 2.0811$, $\theta = 0, \pi$. From equations (2.4) and (2.5), the velocity components are given by

$$v_r = \left[1 - \frac{1}{r^2}\left(\frac{e}{r_0}\right)^2\right]\cos\theta, \quad r > e/r_0, \tag{2.6 a}$$

$$v_r = \frac{2}{r_0 r}\frac{J_1(kr_0 r)}{kJ_0(ke)}\cos\theta, \qquad r \leqslant e/r_0, \tag{2.6 b}$$

and

$$v_\theta = -\left[1 + \frac{1}{r^2}\left(\frac{e}{r_0}\right)^2\right]\sin\theta, \qquad r > e/r_0, \tag{2.7 a}$$

$$v_\theta = -\frac{2}{J_0(ke)}\left[J_0(kr_0 r) - \frac{J_1(kr_0 r)}{kr_0 r}\right]\sin\theta, \quad r \leqslant e/r_0. \tag{2.7 b}$$

In a Cartesian coordinate system (x, y), where x is along the wall with origin beneath the centre of the vortex, and y is measured normal to the wall, the velocity components (u, v) in the respective coordinate directions are related to equations (2.6) and (2.7) by

$$u = v_r \cos\theta - v_\theta \sin\theta, \tag{2.8}$$

$$v = v_r \sin\theta + v_\theta \cos\theta. \tag{2.9}$$

Equations (2.5), (2.8) and (2.9), with equations (2.6) and (2.7), prescribe the inviscid solution for the thick-core vortex above an infinite plane wall, which will be the initial condition for the Navier–Stokes solutions. Note that in non-dimensional variables the wall velocity is $u_\mathrm{w} = -\beta$, where

$$\beta = \alpha/(1 - \alpha). \tag{2.10}$$

3. Boundary-layer formulation

In order to perform a boundary-layer calculation, the slip velocity along the surface is necessary from the inviscid solution in order to provide the external velocity at the outer edge of the boundary layer. It can be shown from equations (2.6) that the inviscid slip velocity along the wall (and thus the mainstream velocity for the boundary layer) is

$$U_\infty(x) = \left[1 - \frac{1}{x^2}\left(\frac{e}{r_0}\right)^2\right], \quad |x| > e/r_0, \tag{3.1 a}$$

$$U_\infty(x) = \frac{2}{r_0|x|}\frac{J_1(kr_0|x|)}{kJ_0(ke)}, \quad |x| \leqslant e/r_0, \quad x \neq 0, \tag{3.1 b}$$

$$U_\infty(x) = \frac{1}{J_0(\lambda)}, \qquad x = 0. \tag{3.1 c}$$

The value of $U_\infty(0)$ in equation (3.1 *c*) is obtained from the general equation (3.1 *b*) for $|x| \leqslant e/r_0$ using the fact that $J_1(z) \sim z/2$ for small z. The mainstream velocity distribution (3.1) for the thick-core vortex is qualitatively similar to that for the rectilinear vortex (see Doligalski *et al.* (1994) for a comparison).

A critical value of the wall speed β (and α) occurs when the wall speed exactly balances the minimum external velocity, which occurs at $x = 0$. From equation (3.1 *c*), $U_{\infty\,\min} = U_\infty(0) = -2.4829$; therefore, the critical values of β and α are $\beta_\mathrm{c} = 2.4829$ and $\alpha_\mathrm{c} = 0.7129$. For $\beta < \beta_\mathrm{c}$, the magnitude of the wall speed is less than $U_{\infty\,\min}$, and the boundary-layer response is dominated by the influence of the adverse pressure gradient imposed by the external flow. For $\beta > \beta_\mathrm{c}$, however, the magnitude of the wall speed is greater than $U_{\infty\,\min}$, and the boundary-layer response is dominated by the rapidly moving wall. It has been found by Degani *et al.* (1998) that unsteady

boundary-layer separation is suppressed for wall speeds β greater than a value that is slightly less than β_c.

The following dimensionless variables are defined in the boundary layer:

$$x = x^*/r_0, \tag{3.2 a}$$

$$\bar{y} = (y^*/r_0)Re^{1/2}, \tag{3.2 b}$$

$$t = \frac{U_0(1-\alpha)t^*}{r_0}, \tag{3.2 c}$$

$$u = \frac{u^*}{U_0(1-\alpha)}, \tag{3.2 d}$$

$$\bar{v} = \frac{v^*}{U_0(1-\alpha)}Re^{1/2}, \tag{3.2 e}$$

where the Reynolds number is defined by $Re = U_0(1-\alpha)r_0/\nu$. Overbars are used on scaled boundary-layer variables to distinguish them from variables used in the Navier–Stokes formulation to follow. The two-dimensional boundary-layer equations for incompressible flow are

$$\frac{\partial u}{\partial t} + u\frac{\partial u}{\partial x} + \bar{v}\frac{\partial u}{\partial \bar{y}} = U_\infty \frac{\mathrm{d}U_\infty}{\mathrm{d}x} + \frac{\partial^2 u}{\partial \bar{y}^2}, \tag{3.3 a}$$

$$\frac{\partial u}{\partial x} + \frac{\partial \bar{v}}{\partial \bar{y}} = 0, \tag{3.3 b}$$

and the boundary conditions are

$$u = -\beta, \quad \bar{v} = 0 \quad \text{at } \bar{y} = 0, \tag{3.4 a}$$

$$u \to U_\infty(x) \quad \text{as } \bar{y} \to \infty. \tag{3.4 b}$$

The flow is initiated in an impulsive start at $t = 0$, followed by formation of a boundary layer that thickens proportional to $t^{1/2}$. Therefore, Rayleigh variables are introduced as follows

$$\zeta = \bar{y}/2t^{1/2}, \tag{3.5 a}$$

$$\Psi = \bar{\psi}/2t^{1/2}, \tag{3.5 b}$$

where $\bar{\psi}$ is the streamfunction defined by $u = \partial\bar{\psi}/\partial\bar{y}$, $\bar{v} = -\partial\bar{\psi}/\partial x$. Substitution of these variables into the governing equations (3.3) gives the following set of equations

$$4t\frac{\partial u}{\partial t} = \frac{\partial^2 u}{\partial \zeta^2} + 2\zeta\frac{\partial u}{\partial \zeta} + 4t\left[\frac{\partial \Psi}{\partial x}\frac{\partial u}{\partial \zeta} - u\frac{\partial u}{\partial x} + U_\infty\frac{\mathrm{d}U_\infty}{\mathrm{d}x}\right], \tag{3.6 a}$$

$$u = \frac{\partial \Psi}{\partial \zeta}, \tag{3.6 b}$$

and the boundary conditions (3.4) become

$$u = -\beta, \quad \Psi = 0 \quad \text{at } \zeta = 0, \tag{3.7 a}$$

$$u \to U_\infty(x) \quad \text{as } \zeta \to \infty. \tag{3.7 b}$$

The initial conditions are obtained by taking equations (3.6) as $t \to 0$ and solving the resulting equations subject to the boundary conditions (3.7). This gives

$$u = (U_\infty + \beta)\,\mathrm{erf}(\zeta) - \beta, \tag{3.8 a}$$

$$\Psi = (U_\infty + \beta)[\zeta\,\mathrm{erf}(\zeta) - \pi^{-1/2}(1 - \mathrm{e}^{-\zeta^2})] - \beta\zeta, \tag{3.8 b}$$

at $t = 0$. The boundary layer at upstream and downstream infinity is not influenced by the presence of the vortex; therefore, the streamwise boundary conditions as $x \to \pm\infty$ are also given by equations (3.8) for all t.

The Eulerian formulation given above is suitable for determining the flow at early times after the impulsive start. However, strong gradients develop in the latter stages of the calculation as an unsteady eruption begins to occur, and it is advantageous to use a Lagrangian formulation of the boundary-layer equations. In the Lagrangian description of the motion, the trajectories of the fluid particles are determined as functions of their initial locations and time. Taking ξ to be the initial streamwise location and η the initial normal location of the fluid particles at some time $t = t_0$, the dependent variables are the streamwise and normal particle positions $x = x(\xi, \eta, t)$ and $y = y(\xi, \eta, t)$, respectively, and the corresponding velocity components $u = u(\xi, \eta, t)$ and $v = v(\xi, \eta, t)$. In Lagrangian coordinates the boundary-layer momentum equation (3.3 a) becomes

$$\frac{\partial u}{\partial t} = U_\infty \frac{\mathrm{d}U_\infty}{\mathrm{d}x} + \left[\frac{\partial x}{\partial \xi}\frac{\partial}{\partial \eta} - \frac{\partial x}{\partial \eta}\frac{\partial}{\partial \xi}\right]^2 u, \tag{3.9 a}$$

where

$$\frac{\partial x}{\partial t} = u. \tag{3.9 b}$$

It is convenient to compute the initial stages of the flow after the impulsive start at $t = 0$ using the Eulerian formulation and then switch over to the Lagrangian formulation at some time $t = t_0$. Therefore, the initial conditions for the Lagrangian calculation are

$$x(\xi, \eta, t) = \xi, \quad u(\xi, \eta, t) = u_0(\xi, \eta) \quad \text{at } t = t_0, \tag{3.10}$$

where $u_0(\xi, \eta)$ is the streamwise velocity distribution at $t = t_0$ from the Eulerian calculation. In the Lagrangian formulation, the boundary conditions at the wall and as the mainstream is approached are

$$u = -\beta \qquad \text{at } \eta = 0, \tag{3.11 a}$$

$$u \to U_\infty(x) \quad \text{as } \eta \to \infty. \tag{3.11 b}$$

The flow at upstream and downstream infinity is plane parallel; therefore, $\bar{y} = \eta$ for all t and from equation (3.8 a) with (3.5 a):

$$u = (U_\infty + \beta)\,\mathrm{erf}\left(\frac{\eta}{2t^{1/2}}\right) - \beta \quad \text{as } \xi \to \pm\infty. \tag{3.12}$$

The boundary-layer equations in both Eulerian and Lagrangian coordinates are solved using methods similar to those described by Peridier *et al.* (1991 a). A coordinate transformation is used to map the semi-infinite domain into a finite domain

and to concentrate grid points near the surface at $\bar{y} = 0$ and near $x = 0$, where the eruption occurs. Starting at $t = 0$, an iteration is initiated on the boundary-layer equations (3.6) in Eulerian coordinates at each time-step in order to obtain the streamwise velocity $u(x, \zeta, t)$ and the streamfunction $\Psi(x, \zeta, t)$. Then at some time $t = t_0$, a Lagrangian calculation is initiated using the results of the Eulerian calculation as the initial conditions. The boundary-layer equations in Lagrangian coordinates (3.9) are solved to obtain the streamwise velocity $u(\xi, \eta, t)$ and particle position $x(\xi, \eta, t)$. The momentum equations in both formulations are solved using a factored alternating-direction-implicit (ADI) method that is second-order accurate in both space and time. The time, t_s, and location of the non-interactive boundary-layer singularity are determined from a solution of the continuity equation, which in Lagrangian coordinates is a first-order linear partial differential equation for the normal particle positions $y(\xi, \eta, t)$ (see Peridier *et al.* 1991*a*).

4. Navier–Stokes formulation

The primary objective of this investigation is to obtain numerical solutions of the Navier–Stokes equations for the flow induced by a thick-core vortex. In a manner similar to that used for the boundary-layer equations, we non-dimensionalize with respect to the normal distance to the vortex centre r_0 and the streamwise velocity at infinity $U_0(1 - \alpha)$, as follows:

$$x = x^*/r_0, \tag{4.1a}$$

$$y = y^*/r_0, \tag{4.1b}$$

$$t = \frac{U_0(1-\alpha)t^*}{r_0}, \tag{4.1c}$$

$$u = \frac{u^*}{U_0(1-\alpha)}, \tag{4.1d}$$

$$v = \frac{v^*}{U_0(1-\alpha)}, \tag{4.1e}$$

$$p = \frac{p^*}{\rho_\infty U_0^2(1-\alpha)^2}. \tag{4.1f}$$

For two-dimensional incompressible flow, the unsteady Navier–Stokes equations in non-dimensional form are

$$\frac{\partial u}{\partial t} + u\frac{\partial u}{\partial x} + v\frac{\partial u}{\partial y} = -\frac{\partial p}{\partial x} + \frac{1}{Re}\left[\frac{\partial^2 u}{\partial x^2} + \frac{\partial^2 u}{\partial y^2}\right], \tag{4.2a}$$

$$\frac{\partial v}{\partial t} + u\frac{\partial v}{\partial x} + v\frac{\partial v}{\partial y} = -\frac{\partial p}{\partial y} + \frac{1}{Re}\left[\frac{\partial^2 v}{\partial x^2} + \frac{\partial^2 v}{\partial y^2}\right], \tag{4.2b}$$

$$\frac{\partial u}{\partial x} + \frac{\partial v}{\partial y} = 0, \tag{4.2c}$$

where the Reynolds number is defined in the same way as in the boundary-layer formulation; $Re = U_0(1 - \alpha)r_0/\nu$. The vortex centre is initially located at $x = 0$, $y = 1$, and the boundary conditions are

$$u = -\beta, \quad v = 0 \quad \text{at } y = 0, \tag{4.3a}$$

$$u \to 1, \quad v \to 0 \quad \text{as } y \to \infty. \tag{4.3b}$$

An alternative to the primitive-variables formulation given by equations (4.2) is the vorticity-streamfunction formulation, where the vorticity is defined by

$$\omega = \frac{\partial v}{\partial x} - \frac{\partial u}{\partial y}, \tag{4.4}$$

and the streamfunction is defined by

$$u = \frac{\partial \psi}{\partial y}, \tag{4.5 a}$$

$$v = -\frac{\partial \psi}{\partial x}. \tag{4.5 b}$$

Taking the derivative of (4.2 *a*) with respect to y and the derivative of (4.2 *b*) with respect to x and subtracting gives the two-dimensional vorticity transport equation:

$$\frac{\partial \omega}{\partial t} + u\frac{\partial \omega}{\partial x} + v\frac{\partial \omega}{\partial y} = \frac{1}{Re}\left[\frac{\partial^2 \omega}{\partial x^2} + \frac{\partial^2 \omega}{\partial y^2}\right]. \tag{4.6}$$

Combining equations (4.4) and (4.5) gives the Poisson equation for the streamfunction:

$$\frac{\partial^2 \psi}{\partial x^2} + \frac{\partial^2 \psi}{\partial y^2} = -\omega. \tag{4.7}$$

The flow is impulsively started at $t = 0$ using the inviscid solution for the thick-core vortex as the initial condition. The streamfunction for the inviscid solution is given by equations (2.5) and the velocity components by equations (2.8) and (2.9) with equations (2.6) and (2.7). The initial vorticity distribution can be obtained by substituting the expression for the streamfunction (2.5) into the Poisson equation (4.7) written in cylindrical coordinates to give

$$\omega(r, \theta) = 0, \qquad r > e/r_0, \tag{4.8 a}$$

$$\omega(r, \theta) = (kr_0)^2 \psi(r, \theta), \quad r \leqslant e/r_0, \tag{4.8 b}$$

at $t = 0$.

The boundary conditions on the streamfunction, velocity components and vorticity at the top and bottom of the domain are

$$\psi = 0, \quad u = -\beta, \quad v = 0 \quad \text{at } y = 0, \tag{4.9 a}$$

$$\psi \to y, \quad u \to 1, \quad v \to 0, \quad \omega \to 0 \quad \text{as } y \to \infty. \tag{4.9 b}$$

At upstream and downstream infinity, the boundary conditions are obtained from equations (4.2 *a*) and (4.6) as $|x| \to \infty$, which gives

$$\frac{\partial u}{\partial t} = \frac{1}{Re}\frac{\partial^2 u}{\partial y^2}, \tag{4.10 a}$$

$$\frac{\partial \omega}{\partial t} = \frac{1}{Re}\frac{\partial^2 \omega}{\partial y^2}. \tag{4.10 b}$$

The solutions to these equations subject to the appropriate boundary conditions are

$$u = (1 + \beta)\,\mathrm{erf}(z) - \beta, \tag{4.11 a}$$

$$\omega = -\omega_{\mathrm{w}}\,\mathrm{erf}(z) + \omega_{\mathrm{w}}, \tag{4.11 b}$$

and the corresponding streamfunction is

$$\psi = (y/z)\{(1+\beta)[z\,\mathrm{erf}(z) - \pi^{-1/2}(1-\mathrm{e}^{-z^2})] - \beta z\}, \tag{4.11 c}$$

where $z = y(Re/t)^{1/2}/2$. Here, ω_w is the vorticity at the wall as $|x| \to \infty$.

Just as in the boundary-layer formulation, it is advantageous to incorporate coordinate transformations that map the semi-infinite physical domain into a finite computational domain. This is done using the following transformations

$$\hat{x} = \frac{2}{\pi}\arctan\left(\frac{x-x_0}{a}\right), \tag{4.12 a}$$

$$\hat{y} = \frac{2}{\pi}\arctan\left(\frac{y}{b}\right), \tag{4.12 b}$$

which maps $x = \infty$ to $\hat{x} = 1$ and $x = -\infty$ to $\hat{x} = -1$. The transformations concentrate mesh points near $x = x_0$, the streamwise location of the eruption, and $y = 0$, the surface, with the parameters a and b determining the degree of focusing of grid points. Applying these transformations to the vorticity transport equation (4.6) gives

$$\frac{\partial\omega}{\partial t} = R(\hat{x})\frac{\partial^2\omega}{\partial\hat{x}^2} + S(\hat{y})\frac{\partial^2\omega}{\partial\hat{y}^2} + G(\hat{x},\hat{y})\frac{\partial\omega}{\partial\hat{x}} + H(\hat{x},\hat{y})\frac{\partial\omega}{\partial\hat{y}}, \tag{4.13 a}$$

where

$$R(\hat{x}) = (1/Re)\Gamma_x^2(\hat{x}), \tag{4.13 b}$$

$$S(\hat{y}) = (1/Re)\Gamma_y^2(\hat{y}), \tag{4.13 c}$$

$$G(\hat{x},\hat{y}) = (1/Re)\Gamma_x(\hat{x})\Gamma_x'(\hat{x}) - \Gamma_x(\hat{x})u(\hat{x},\hat{y}), \tag{4.13 d}$$

$$H(\hat{x},\hat{y}) = (1/Re)\Gamma_y(\hat{y})\Gamma_y'(\hat{y}) - \Gamma_y(\hat{y})v(\hat{x},\hat{y}). \tag{4.13 e}$$

A prime denotes differentiation with respect to the indicated variable, and the Γ coefficients are given by

$$\Gamma_x(\hat{x}) = (1/\pi a)[1+\cos(\pi\hat{x})], \tag{4.14 a}$$

$$\Gamma_y(\hat{y}) = (1/\pi b)[1+\cos(\pi\hat{y})]. \tag{4.14 b}$$

Applying the transformations (4.12) to the Poisson equation for the streamfunction (4.7) gives

$$A(\hat{x})\frac{\partial^2\psi}{\partial\hat{x}^2} + B(\hat{x})\frac{\partial\psi}{\partial\hat{x}} + C(\hat{y})\frac{\partial^2\psi}{\partial\hat{y}^2} + D(\hat{y})\frac{\partial\psi}{\partial\hat{y}} = E(\hat{x},\hat{y}), \tag{4.15 a}$$

where

$$A(\hat{x}) = \Gamma_x^2(\hat{x}), \tag{4.15 b}$$

$$B(\hat{x}) = \Gamma_x(\hat{x})\Gamma_x'(\hat{x}), \tag{4.15 c}$$

$$C(\hat{y}) = \Gamma_y^2(\hat{y}), \tag{4.15 d}$$

$$D(\hat{y}) = \Gamma_y(\hat{y})\Gamma_y'(\hat{y}), \tag{4.15 e}$$

$$E(\hat{x},\hat{y}) = -\omega(\hat{x},\hat{y}). \tag{4.15 f}$$

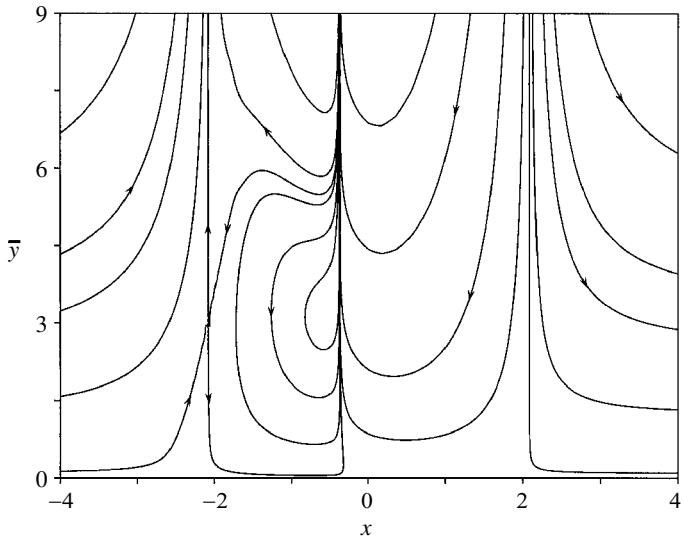

Figure 3. Streamlines at $t = t_s = 1.402$ from the non-interactive boundary-layer calculation.

The vorticity transport equation (4.13) is solved using the same factored ADI algorithm used to solve the streamwise momentum equations in the boundary-layer problem. The algorithm incorporates upwind–downwind differencing of the first-order derivatives and uses the Crank–Nicolson technique for marching in time; the algorithm is second-order accurate in both space and time. The boundary condition for the vorticity at the wall ($y = 0$) is obtained using Jensen's method, which gives a second-order accurate estimate for the vorticity at the surface. The Poisson equation (4.15) for the streamfunction is discretized using central differences and solved using a fast direct solver for block tridiagonal systems.

5. Boundary-layer results

Before discussing solutions of the Navier–Stokes equations, it is instructive to consider solutions of the non-interactive boundary-layer equations induced by the thick-core vortex. These boundary-layer solutions correspond to the limit problem $Re \rightarrow \infty$, representing the first stage of unsteady separation; therefore, they should compare well with the Navier–Stokes solutions for finite Reynolds numbers prior to the onset of interaction. Here, results are given for the case with $\beta = 0$ corresponding to the situation in which the strength of the vortex is sufficient to exactly balance the uniform flow, and the vortex remains stationary relative to the surface. This choice is somewhat arbitrary as it is expected that all solutions obtained with $\beta < \beta_c$ will be qualitatively similar. The boundary-layer results shown here have been obtained on a grid with 301 points in the streamwise direction and 151 points in the direction normal to the surface. The stretching parameters are $a = 1.25$, $b = 1.25$, and the time-step is reduced from $\Delta t = 0.001$ at the start of the computation to $\Delta t = 0.0001$ prior to the singularity. Solutions have been obtained on various grids and with different time-steps to ensure that the results shown are grid independent.

After an impulsive start at $t = 0$, the boundary-layer solution exhibits a secondary recirculation region at approximately $t = 0.4$ that grows in extent normal to the sur-

face as time increases. This secondary recirculation region results from the locally adverse streamwise pressure gradient induced by the thick-core vortex. At approximately $t = 1.3$, a kink begins to form in the streamlines on the right-hand side of the recirculation region; this is rapidly followed by the formation of a very sharp spike and an eventual singularity at $t = t_s = 1.402$, as shown in figure 3. These results for the thick-core vortex are qualitatively the same as those obtained by Peridier *et al.* (1991*a*) for the rectilinear vortex and only differ in the times at which the above-mentioned events occur within the boundary-layer flow.

6. Navier–Stokes solutions

Boundary-layer singularities do not occur in the Navier–Stokes equations; therefore, we would expect that solutions of the full Navier–Stokes equations at high enough Reynolds numbers would exhibit the trends observed as a singularity is approached in the reduced set of equations, but not the singularity itself. Detailed results will be given for the case with $\beta = 0$ and $Re = 10^5$. Note that this Reynolds number is based on a local length-scale, i.e. the height of the vortex above the wall; therefore, if it was based on a global length-scale, such as the chord length of an aerofoil with the vortex being the dynamic–stall vortex, the Reynolds number would be approximately one order of magnitude larger. In computing the solution, considerable effort has been devoted to ensuring that the results are grid independent and that they compare well with solutions of the boundary-layer equations at early times. Results are given here from a calculation on a 301×301 grid with the transformation parameters given by $a = 1.0$, $b = 0.05$ and $x_0 = -0.5$. Note that b is small in order to adequately resolve the boundary layer. The time-step used was $\Delta t = 0.0005$.

The primary objective of this investigation is to identify the various stages of unsteady separation within the context of the Navier–Stokes solutions and to determine what physical effect becomes important prior to the time-scale on which the *first* interactive stage governs. In order to evaluate the relative importance of various physical processes, quantities such as the streamwise pressure gradient along the surface, the wall shear stress, the normal pressure gradient and the streamwise diffusion term have been evaluated within the boundary layer as the calculation progressed. Because the streamwise pressure gradient within the boundary layer is imposed by the steady inviscid outer flow and the normal pressure gradient within the boundary layer is zero during the non-interactive stage of the flow, the streamwise pressure gradient along the surface does not change until interaction between the viscous boundary layer and the inviscid outer flow begins, signalling the onset of the second asymptotic stage (see figure 1). Applying the streamwise momentum equation from the Navier–Stokes equations on the surface ($u = \text{const.}$, $v = 0$) and writing in terms of vorticity, the streamwise pressure gradient along the surface may be determined from

$$\frac{\partial p}{\partial x} = \frac{1}{Re} \Gamma_y(\hat{y}) \frac{\partial \omega}{\partial \hat{y}}. \tag{6.1}$$

In addition to indicating the onset of interaction, the streamwise pressure gradient, along with the wall shear stress, signal when the interactive stage breaks down. Recall that the interacting boundary-layer singularity of Smith (1988) is characterized by singularities in these two quantities. In order to determine when the third stage

of unsteady separation begins, the maximum value of the normal pressure gradient within the boundary layer has been determined as the solution evolves. The normal pressure gradient was found by evaluating the momentum equation in the normal direction (4.2 *b*) solved for $\partial p/\partial y$. The magnitude of the streamwise diffusion term in the momentum equation was also evaluated; as expected, however, it is not found to be important for the duration of the current calculations.

The first stage of unsteady separation is the non-interactive stage and is governed by the classical boundary-layer equations. Therefore, the solutions of the Navier–Stokes equations should agree with the solutions discussed in the previous section. Indeed, during the initial stage of the calculation, numerical solutions of the Navier–Stokes equations (scaled to match the boundary-layer scale) match very closely with those from the boundary-layer calculation up until approximately $t = 0.8$, which is well after formation of the recirculation region at approximately $t = 0.4$. Until $t \approx 0.8$, the distribution of streamwise pressure gradient along the surface remains essentially the same and is as shown in figure 4 at $t = 0.7$. At approximately $t = 0.8$, the streamwise pressure gradient along the surface begins to change in the region where the streamlines abruptly change direction in order to pass over the secondary recirculation region; this may be observed at $t = 0.9$ in figure 4. This event signals that interaction has begun between the viscous boundary layer and the inviscid outer flow. The streamlines at an even later time, however, do not exhibit a spike (see figure 5*a*), which was thought to be a precursor to the onset of interaction. Note that in figure 5 the normal scale has been greatly expanded such that for the Reynolds number considered, the scale exactly matches that in figure 3 for the boundary-layer calculation (compare equations (3.2 *b*) and (4.1 *b*)). As shown in figure 4, the spike in pressure gradient continues to grow in amplitude, and at approximately $t = 1.1$ the wall shear stress begins to develop a spike at the same streamwise location. Recall that it is these quantities that become singular in the interacting boundary-layer singularity of Smith (1988). The streamwise pressure gradient and wall shear from the Navier–Stokes calculation are shown in figure 4 at $t = 1.3$, about the time at which the interacting boundary-layer singularity would be likely to occur. As shown in figure 5*b*, it is at approximately $t = 1.1$ that the streamlines develop a kink on the right-hand side of the secondary recirculation region; note that this is prior to the time at which this begins to occur in the boundary-layer solution (i.e. $t \approx 1.3$). This is consistent with the results of Peridier *et al.* (1991*b*), who found that the inclusion of interaction hastens the unsteady separation process. As time increases, this kink develops into a spike (figure 5*c*) that erupts away from the surface, as shown in figure 5*d*. Note that the spike has a finite width in the streamwise direction in contrast to the non-interactive boundary-layer solution, in which the spike formally goes to zero thickness as the singularity is approached (cf. figure 3).

It is expected that normal pressure gradients will become important within the boundary layer at some time prior to that at which the interacting boundary-layer singularity would occur ($t_{\mathrm{sI}} \approx 1.3$). The maximum value of the normal pressure gradient within the boundary layer from the Navier–Stokes solution is shown at various times in figure 6. Note that these values of the normal pressure gradient are in terms of the boundary-layer variable, i.e. $\partial p/\partial \bar{y} = Re^{-1/2}\partial p/\partial y$. Observe that, at approximately $t = 1.2$, the magnitude of the normal pressure gradient begins to rise dramatically and becomes an $O(1)$ influence locally within the boundary layer. This sudden rise in the normal pressure gradient appears to follow the formation of the

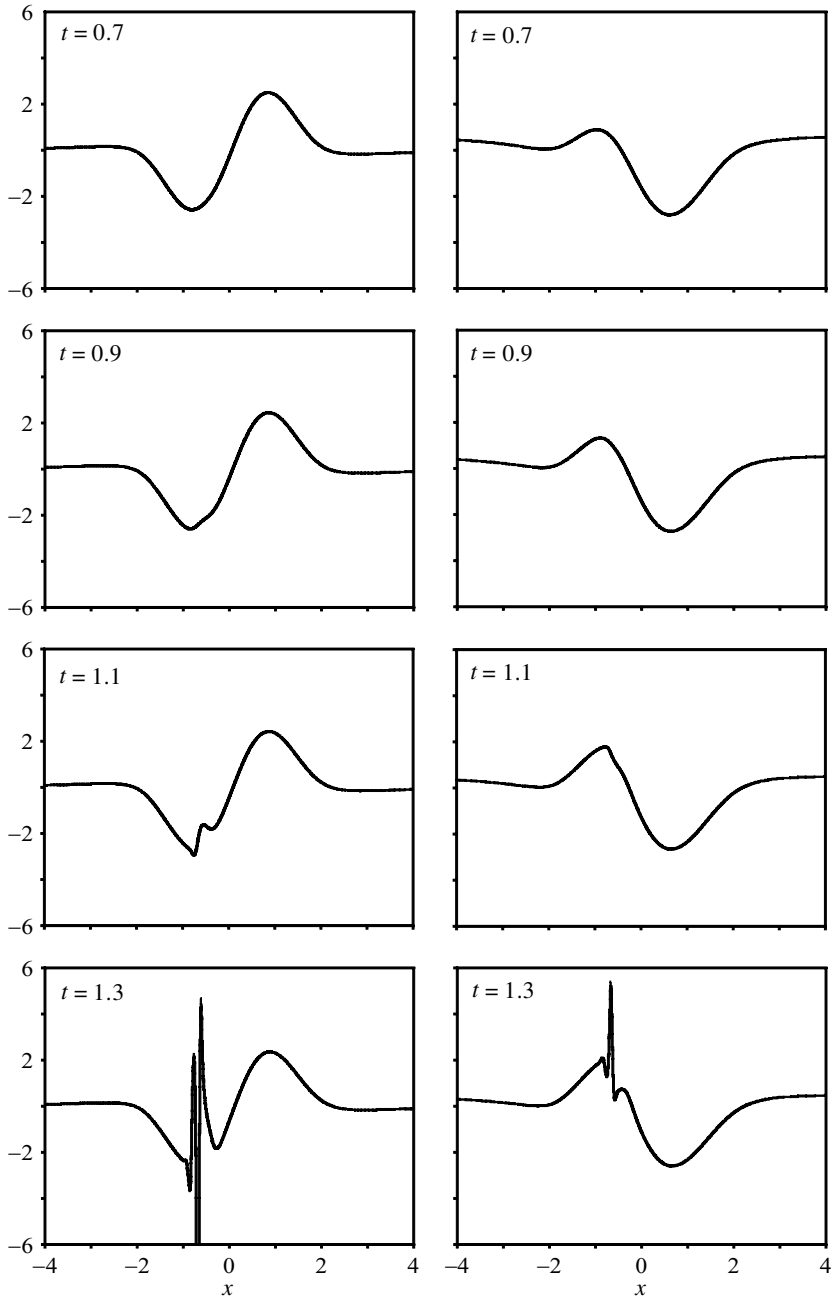

Figure 4. Streamwise pressure gradient $\partial p/\partial x$ along the surface (left) and wall shear stress τ_w (right) at various times from the Navier–Stokes calculation.

spike in the streamlines that begins at approximately $t = 1.1$, and the location of the maximum in normal pressure gradient occurs just above the growing spike. As predicted by Hoyle *et al.* (1991), the normal pressure gradient relieves the interacting boundary-layer singularity, which in the Navier–Stokes solutions is characterized by

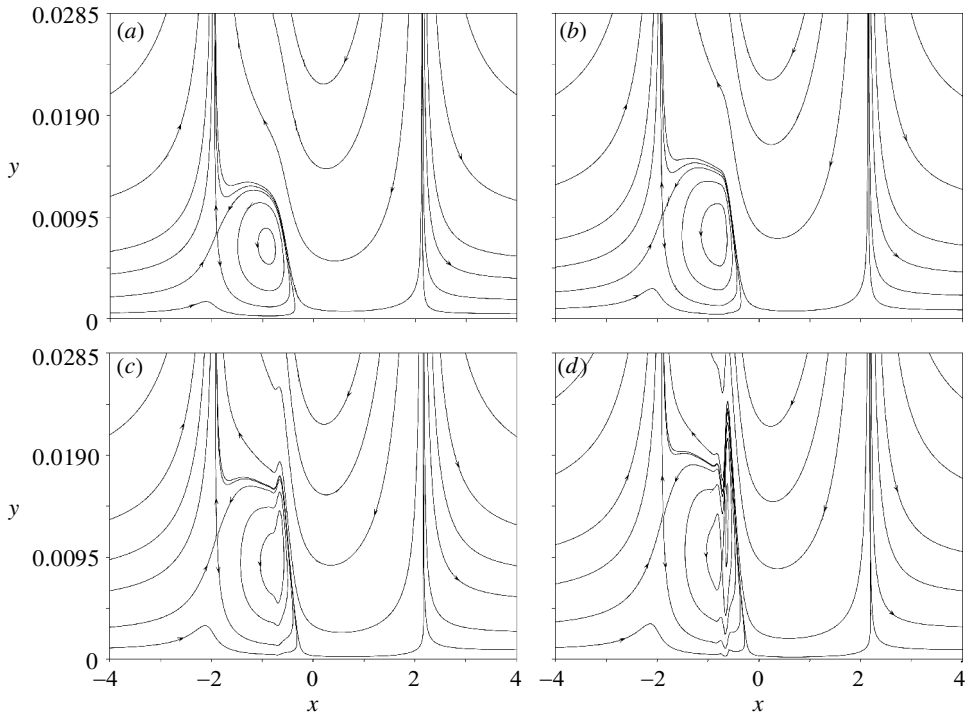

Figure 5. Streamlines within the boundary layer from the Navier–Stokes calculation for $Re = 10^5$. (*a*) $t = 1.0$, (*b*) $t = 1.1$, (*c*) $t = 1.2$, (*d*) $t = 1.3$.

large spikes in the streamwise pressure gradient and the wall shear stress, which are evident at $t = 1.3$ in figure 4. It is also approximately at this time that the secondary recirculating eddy splits for the first time, as shown in figure 5*d*; it then splits again at $t \approx 1.4$ (not shown). Each time the eddy splits, another spike forms and begins to grow normal to the surface; the early stages of this process can be seen in figure 5*d* just to the left of the primary eddy. This eddy splitting has also been observed in the interacting boundary-layer results of Peridier *et al.* (1991*b*). The present calculations were terminated at $t = 1.5$, at which time the flow is very complex due to the multiple eddies and spikes and is difficult to resolve.

In order to ensure that these results for $Re = 10^5$ are representative, solutions have also been obtained for $Re = 10^3$ and $Re = 10^4$ but are not shown here. The solution for $Re = 10^4$ is qualitatively the same as that for $Re = 10^5$ and differs only in the times at which certain events begin to occur. The early stages of the Navier–Stokes solution match with the non-interactive boundary-layer solution, but the large-scale viscous–inviscid interaction begins earlier and the spike in streamwise pressure gradient grows less rapidly than for the case with $Re = 10^5$. In addition, the spike in the streamlines—and, thus, the small-scale interaction—are wider in the streamwise direction and grow less rapidly normal to the surface. The results for $Re = 10^3$ proceed as for the higher Reynolds numbers, except that no spike forms at all; therefore, there is no small-scale interaction. Instead, the recirculation region continues to grow and eventually interacts with the primary vortex; the large-scale viscous–inviscid interaction begins at approximately $t = 0.7$. Evidently, the

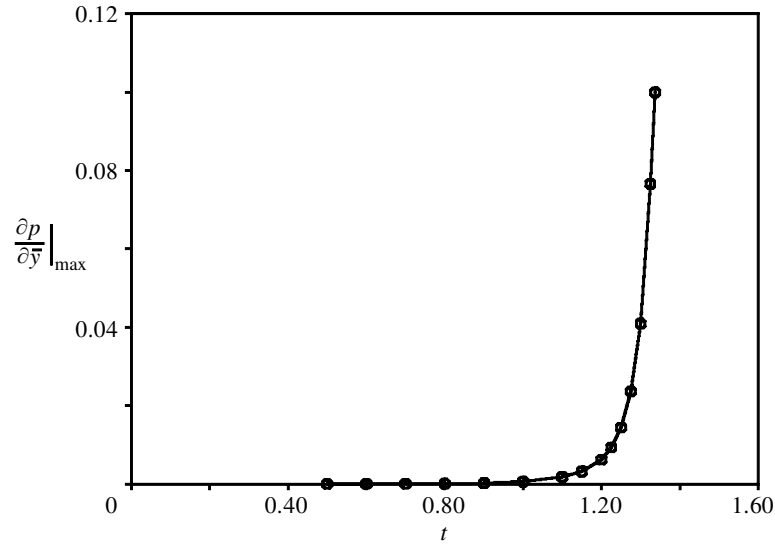

Figure 6. Variation of the maximum value of the normal pressure gradient $\partial p/\partial \bar{y}$ with time within the boundary layer from the Navier–Stokes calculation.

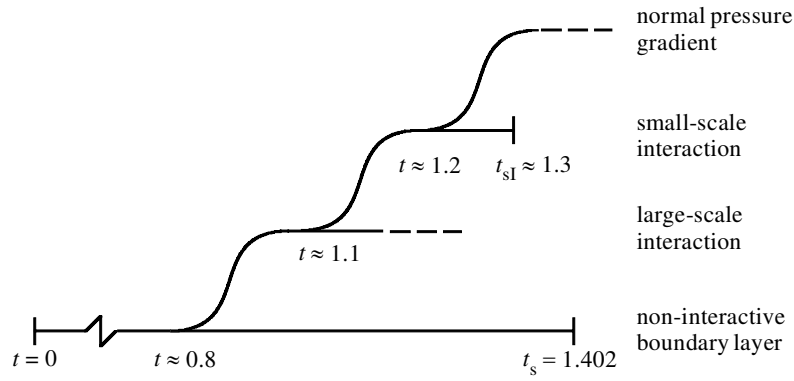

Figure 7. Summary of the times at which significant events occur in the non-interactive boundary-layer calculation and the Navier–Stokes solution for $Re = 10^5$.

streamwise extent and normal growth rate of the spike have some Reynolds number dependence that results in a weaker spike as the Reynolds number is reduced to the point where for $Re = 10^3$, no spike forms at all.

7. Discussion

Solutions of the unsteady boundary-layer and Navier–Stokes equations have been obtained for the flow induced by a thick-core vortex above an infinite plane surface in a uniform flow. The non-interactive boundary-layer results and those from the Navier–Stokes calculation with $Re = 10^5$ are summarized in figure 7. In the non-interactive boundary-layer calculation, a secondary recirculation region begins to form at approximately $t = 0.4$ and grows in streamwise and normal extent leading to the formation of a sharp spike in the streamlines beginning at approximately $t = 1.3$

followed by a singularity at $t = t_s = 1.402$. At a time much earlier than the non-interactive singularity, at approximately $t = 0.8$, a local change in the streamwise pressure gradient along the surface becomes evident in the Navier–Stokes solutions, indicating that viscous–inviscid interaction is becoming important locally. This interaction begins well before formation of the spike in the streamlines and appears to occur over a larger streamwise scale than is suggested by the asymptotic theory; therefore, it is referred to here as the *large-scale* interaction and is represented by the second tier in figure 7. It is apparently the development of a locally strong outflow normal to the surface that initiates this large-scale interaction; this outflow begins to develop within the boundary layer immediately upstream (to the right) of the secondary recirculation region as the flow changes directions abruptly in order to pass over the eddy, which acts as a barrier. At approximately $t = 1.1$, a spike begins to develop on the upstream side of the secondary recirculation region. Note that this is prior to the formation of the spike in the non-interactive boundary-layer solution, which occurs at $t \approx 1.3$, suggesting that the large-scale interaction hastens the initial formation of the spike. It is postulated here that the growth of the spike leads to a *small-scale* interaction that occurs on scales that are distinct from the large-scale interaction and are presumably given by the *first* interactive stage of Elliott *et al.* (1983). The small-scale interactive stage ends at approximately $t = t_{sI} \approx 1.3$, when both the streamwise pressure gradient and wall shear stress become very large, which is indicative of the interacting boundary-layer singularity (Smith 1988). Note that this occurs prior to the time at which the non-interactive singularity occurs, i.e. $t_{sI} < t_s$, in agreement with Peridier *et al.* (1991*b*), who found that interaction accelerates the eruptive process. Prior to the time at which the interacting boundary-layer singularity would occur, normal pressure gradients become important locally within the boundary layer above the growing spike. This occurs at approximately $t = 1.2$ and is represented by the top tier in figure 7.

In summary, the sequence of events exhibited in high-Reynolds-number solutions of the Navier–Stokes equations for vortex-induced separation appear to corroborate the first three stages in the theoretical description of unsteady separation. Although the general sequence occurs as predicted, the viscous–inviscid interaction process evolves somewhat differently. It had been thought that the formation of a spike within the context of non-interacting boundary-layer theory was a necessary precursor to the onset of interaction. Recall that the initial condition for the so-called *first* interactive stage is the terminal boundary-layer solution, which is a similarity solution for the boundary-layer flow within the spike as the singularity is approached (Elliott *et al.* 1983; Cassel *et al.* 1996); therefore, the *first* interactive stage presumes that the spike has formed prior to its inception. However, numerical solutions of the Navier–Stokes equations show that viscous–inviscid interaction becomes an important mechanism in the evolution of unsteady separation well before the formation of such a spike. It appears that over some Reynolds number range, for which $Re = 10^5$ is representative, interaction occurs over two distinct sets of spatial and temporal scales. A large-scale viscous–inviscid interaction occurs well before the formation of a spike in the streamlines, then the growth of the spike provokes a subsequent small-scale interaction leading to the introduction of normal pressure gradients within the boundary layer. The existence of the large-scale interaction may be the reason for the unusual breakdown of the *first* interactive stage observed by Cassel *et al.* (1996). In hindsight, these results appear to be consistent with the interacting boundary-layer

results of Peridier *et al.* (1991*b*), in that interaction must begin prior to formation of a spike because the interacting boundary-layer singularity time t_{sI} is in some cases prior to the time at which a spike begins to form in the non-interactive calculation (cf. Peridier *et al.* 1991*a*).

These Navier–Stokes solutions suggest that in terms of the nature of the interaction between the viscous boundary layer and the inviscid outer flow, the unsteady separation process evolves somewhat differently in three distinct Reynolds number regimes. At high Reynolds numbers (e.g. $Re \to \infty$), initially governed by solutions of the non-interactive boundary-layer equations, the flow develops a very sharp spike that evolves toward a singularity. This sharp spike provokes a small-scale interaction with the outer inviscid flow, referred to in Cassel *et al.* (1996) as the *first* interactive stage. At moderate Reynolds numbers (e.g. $Re = 10^4$ and $Re = 10^5$), the flow develops as in the high-Reynolds-number case, except that large-scale interaction begins prior to the formation of the spike; the spike then provokes the small-scale interaction. The results obtained in this investigation are believed to be representative of this moderate-Reynolds-number regime. At low Reynolds numbers (e.g. $Re = 10^3$), large-scale interaction begins just as for the moderate-Reynolds-number case; however, no spike forms at later times and there is no small-scale interaction. Most previous numerical solutions of the Navier–Stokes equations involving unsteady separation fall within this regime (see, for example, Choudhuri & Knight 1996). The influence of the large-scale interaction diminishes as the Reynolds number is increased due to the decreasing displacement thickness, i.e. $\delta^* = O(Re^{-1/2})$. In the limit as Reynolds number goes to infinity, the displacement thickness is still $O(1)$ on the boundary-layer scale and no large-scale interaction occurs. The small-scale interaction, on the other hand, diminishes with decreasing Reynolds numbers as the spike becomes wider in the streamwise direction and has a slower growth rate. Recall that the Reynolds number used here is defined based on local quantities relative to the vortex; therefore, it would be significantly larger if based on a macroscopic length-scale, such as the cord length of an aerofoil.

From the Navier–Stokes solutions obtained here, it has not been possible to determine the upper limit of the moderate-Reynolds-number regime, in other words the maximum Reynolds number at which both the large-scale and small-scale interactions occur. One would expect to see the time at which the large-scale interaction begins, e.g. $t \approx 0.8$ for $Re = 10^5$, increase with increasing Reynolds number until a Reynolds number is reached at which no large-scale interaction occurs prior to the time at which the spike forms, i.e. $t \approx 1.3$ in the non-interactive case. Based on the results for Reynolds numbers up to $Re = 10^5$, this increase in time is very small, suggesting that the Reynolds number dividing the moderate from the high Reynolds number regimes is very high, possibly much higher than is of practical interest.

The conclusion that a large-scale interaction occurs much earlier than the so-called *first* interactive stage, at least over a certain range of Reynolds numbers, has several consequences for our understanding of unsteady separation. First, because the large-scale interaction begins prior to the appearance of a spike, it appears that the terminal boundary-layer solution is never reached for flows in the moderate-Reynolds-number regime, suggesting that the terminal solution is not as generic a structure as previously thought. Recall that one of the surprising features of the terminal solution is that it is independent of the form of the adverse pressure gradient that initiates the eruptive process. These results would also appear to have

significant consequences for the possible instabilities that have been identified in the non-interacting boundary-layer equations (see, for example, Smith & Elliott 1985; Cowley *et al*. 1985; Bhaskaran *et al*. 1995). These instabilities tend to have relatively slow growth rates; therefore, they may not have sufficient time to develop prior to breakdown of the non-interactive stage. Because interaction becomes important much earlier than previously thought, these non-interactive instabilities have even less time to develop prior to the onset of interaction.

This work was supported by the National Research Council Postdoctoral Fellowship Program and the US Army Research Office under grant no. DAAG55-98-1-0384. I thank Professor F. T. Smith for discussions regarding this work and Mr A. V. Obabko, who refined some of the calculations. I also honour Sir James Lighthill, who I had the privilege of meeting for the first time only days before his untimely death. He was often at the forefront of new developments in fluid dynamics and provided inspiration for many who followed him and his work over his long and fruitful career.

References

Abramowitz, M. & Stegun, I. A. 1964 *Handbook of mathematical functions*. New York: Dover.

Batchelor, G. K. 1967 *An introduction to fluid dynamics*. Cambridge University Press.

Bhaskaran, R., Smith, F. T. & Timoshin, S. N. 1995 The appearance of boundary-layer instabilities as a velocity minimum develops. *Proc. R. Soc. Lond.* A **451**, 331–339.

Brinkman, K. W. & Walker, J. D. A. 1996 Breakup and instability in a high Reynolds number flow. AIAA paper 96-2156.

Cassel, K. W., Smith, F. T. & Walker, J. D. A. 1996 The onset of instability in unsteady boundary-layer separation. *J. Fluid Mech.* **315**, 223–256.

Choudhuri, P. G. & Knight, D. D. 1996 Effects of compressibility, pitch rate, and Reynolds number on unsteady incipient leading-edge boundary-layer separation over a pitching airfoil. *J. Fluid Mech.* **308**, 195–217.

Cowley, S. J., Hocking, L. M. & Tutty, O. R. 1985 The stability of solutions of the classical unsteady boundary-layer equations. *Phys. Fluids* **28**, 441–443.

Degani, A. T., Walker, J. D. A. & Smith, F. T. 1998 Unsteady separation past moving surfaces. *J. Fluid Mech.* **375**, 1–38.

Dodia, B., Doorly, D. J. & Smith, F. T. 1997 Computational modeling of unsteady boundary layer processes. AIAA paper 97-1834.

Doligalski, T. L. & Walker, J. D. A. 1984 The boundary layer induced by a convected two-dimensional vortex. *J. Fluid Mech.* **139**, 1–28.

Doligalski, T. L., Smith, C. R. & Walker, J. D. A. 1994 Vortex interactions with walls. *A. Rev. Fluid Mech.* **26**, 573–616.

Ece, M. C., Walker, J. D. A. & Doligalski, T. L. 1984 The boundary layer on an impulsively started rotating and translating cylinder. *Phys. Fluids* **27**, 1077–1089.

Elliott, J. W., Cowley, S. J. & Smith, F. T. 1983 Breakdown of boundary layers: (i) on moving surfaces; (ii) in semi-similar unsteady flow; (iii) in fully unsteady flow. *Geophys. Astrophys. Fluid Dynamics* **25**, 77–138.

Hoyle, J. M. & Smith, F. T. 1994 On finite-time break-up in three-dimensional unsteady interacting boundary layers. *Proc. R. Soc. Lond.* A **447**, 467–492.

Hoyle, J. M., Smith, F. T. & Walker, J. D. A. 1991 On sublayer eruption and vortex formation. *Comput. Phys. Commun.* **65**, 151–157.

Koumoutsakos, P. & Leonard, A. 1995 High-resolution simulations of the flow around an impulsively started cylinder using vortex methods. *J. Fluid Mech.* **296**, 1–38.

Li, L., Walker, J. D. A., Bowles, R. I. & Smith, F. T. 1998 Short-scale break-up in unsteady interactive layers: local development of normal pressure gradients and vortex wind-up. *J. Fluid Mech.* **374**, 335–378.

Orlandi, P. 1990 Vortex dipole rebound from a wall. *Phys. Fluids* A **2**, 1429–1436.

Peridier, V. J., Smith, F. T. & Walker, J. D. A. 1991*a* Vortex-induced boundary-layer separation. Part 1. The unsteady limit problem $Re \rightarrow \infty$. *J. Fluid Mech.* **232**, 99–131.

Peridier, V. J., Smith, F. T. & Walker, J. D. A. 1991*b* Vortex-induced boundary-layer separation. Part 2. Unsteady interacting boundary-layer theory. *J. Fluid Mech.* **232**, 133–165.

Smith, F. T. 1988 Finite-time break-up can occur in any unsteady interacting boundary layer. *Mathematika* **35**, 256–273.

Smith, F. T. & Elliott, J. W. 1985 On the abrupt turbulent reattachment downstream of leading-edge laminar separation. *Proc. R. Soc. Lond.* A **401**, 1–27.

Van Dommelen, L. L. 1981 Unsteady boundary-layer separation. PhD thesis, Cornell University, New York, USA.

Van Dommelen, L. L. & Shen, S. F. 1980 The spontaneous generation of the singularity in a separating laminar boundary layer. *J. Comput. Phys.* **38**, 125–140.

Van Dommelen, L. L. & Shen, S. F. 1982 The genesis of separation. In *Numerical and physical aspects of aerodynamic flows* (ed. T. Cebeci), pp. 293–311. Springer.

Walker, J. D. A. 1978 The boundary layer due to a rectilinear vortex. *Proc. R. Soc. Lond.* A **359**, 167–188.